Biomaterials 76 (2016) 102–114

Contents lists available at ScienceDirect

Biomaterials

journal homepage: www.elsevier.com/locate/biomaterials

Attempted caveolae-mediated phagocytosis of surface-fixed micro-pillars by human osteoblasts

Caroline Moerke, Petra Mueller, Barbara Nebe*

University Medical Center Rostock, Dept. of Cell Biology, Rostock, Germany

ARTICLE INFO

Article history:
Received 1 July 2015
Received in revised form
30 September 2015
Accepted 14 October 2015
Available online 23 October 2015

Keywords:
Actin
Caveolae
Micro-structure
Micro-particles
Osteoblast
Phagocytosis

ABSTRACT

Cells are sensitive to their underlying micro- and nano-topography, but the complex interplay is not completely understood especially if sharp edges and ridges of stochastically modified surfaces interfere with an attached cell body. Micro-topography offers cues that evoke a large range of cell responses e.g. altered adhesion behavior and integrin expression resulting in disturbed cell functions. In this study, we analyzed why osteoblastic cells mimic the underlying geometrical micro-pillar structure (5 × 5 × 5 μm, spacing of 5 μm) with their actin cytoskeleton. Interestingly, we discovered an attempted caveolae-mediated phagocytosis of each micro-pillar beneath the cells, which was accompanied by increased intracellular reactive oxygen species (ROS) production and reduced intracellular ATP levels. This energy consuming process hampered the cells in their function as osteoblasts at the interface. The raft-dependent/caveolae-mediated phagocytic pathway is regulated by diverse cellular components including caveolin-1 (Cav-1), cholesterol, actin cytoskeleton as well as actin-binding proteins like annexin A2 (AnxA2). Our results show a new aspect of osteoblast–material interaction and give insight into how cells behave on extraordinary micro-structures. We conclude that stochastically structured implants used in orthopedic surgery should avoid any topographical heights which induce phagocytosis to prevent their successful ingrowth.

1. Introduction

A permanent implant should establish a lifelong anchorage in the surrounding bone; for this purpose it is essential to establish a mechanically solid interface with complete fusion of the material's surface and the native bone tissue. Successful orthopedic implant osseointegration relies on the fast formation of bone tissue at the implant surface, but inadequate bony fixation can lead to fibrous tissue formation at the bone-implant interface. Improved fixation and consequently successful ingrowth into the native bone can be achieved by accelerating the onset and rate of immediate cell attachment and proliferation [1].

Material surface topography is known to effect cellular processes like adhesion, spreading, proliferation and production of extracellular matrix (ECM) proteins, consequently cell behavior and cell fate [1,2]. Osseointegration is enhanced on rougher surfaces rather than on smooth ones, but it is also accompanied by changes in the cell physiology, such as the integrin expression [3,4]. The complex connections of the cell-material interactions are not completely understood despite increasing cell biological studies. New implant design strategies pursue the development of new bioactive surfaces evoking cellular responses which promote osseointegration [1].

For the investigation of topography-induced cell changes, regular geometric micro-pillared structures were used as artificial surfaces, extending the work of stochastic surface models [4,5] with the advantage of constant topography variables. Human MG-63 osteoblast-like cells have an integrin subunits profile similar to primary human osteoblasts and have been considered applicable for studying initial cell attachment to surfaces [6]. Interestingly, MG-63 growing on micro-pillar structures showed an actin cytoskeleton which was clustered as local spots around the pillar edges instead of the stress fiber arrangement normally found on planar surfaces. This altered cell architecture resulted in a decreased synthesis of the extra-cellular matrix (ECM) proteins collagen-I (Col1) and bone sialo protein (BSP), accompanied by a reduced β3-integrin expression, the adhesion receptor for BSP [2]. This indicates that the given surface micro-topography strongly affects

* Corresponding author. University Medical Center Rostock, Department of Cell Biology, Schillingallee 69, D-18057 Rostock, Germany.
E-mail address: barbara.nebe@med.uni-rostock.de (B. Nebe).

http://dx.doi.org/10.1016/j.biomaterials.2015.10.030

with cell physiology. But the modes of action of this typical surface-mimicry of the cell's actin of the underlying geometry were still unexplained. Although the synthesis of ECM proteins was significantly disturbed after 24 h, the phosphorylation state of central signaling proteins (e.g. protein kinase B, AKT and glycogen synthase kinase 3, GSK3) remained unaltered on the micro-pillars [7]. Because osteoblasts are able to uptake nano- and micro-particles [8,9] we argued that cells on micro-pillars (5×5×5 μm in size) try to phagocytize these protruding fixed components on the titanium surface by a caveolae-mediated phagocytosis.

Phagocytosis is a specific form of endocytosis involving the actin-dependent internalization of large particles [10]. Caveolae are 50–80 nm diameter cholesterol- and sphingolipid-rich plasma membrane invaginations considering a subdomain of plasma membrane micro-domains which are called lipid rafts. In the caveolae/lipid raft micro-domains, multiple signaling molecules have been localized which are involved in various cellular processes including phagocytosis [11,12] and the transduction of cell surface signals [13].

The raft-dependent/caveolae-mediated phagocytic pathway is regulated by diverse cellular components including caveolin-1 (Cav-1), cholesterol and the actin cytoskeleton, as well as actin-binding proteins like annexin A2 (AnxA2) [12,14]. Cav-1 is the major component of caveolae and, by binding to cholesterol, is essential for the formation and stabilization of caveolar vesicles [11]. This work shows an attempted caveolae-mediated phagocytosis of the fixed titanium-coated micro-pillars (5 × 5 × 5 μm in size) by osteoblast-like cells.

2. Materials and methods

2.1. Titanium surfaces

Periodically micro-textured samples (size 1 cm^2) with regular cubic pillar geometry on the surface having a dimension of 5×5×5 μm in width × length × height and 5 μm in spacing (P−5×5) were used throughout the experiments. In addition micro-pillars with the dimensions 1×1×1 μm in width × length × height and 1 μm spacing (P − 1 × 1 × 1); 2×2×5 μm and 2 μm spacing (P−2×2×5) as well as 3×3×5 μm and 3 μm spacing (P−3×3×5) were used. As controls unstructured, plane silicon wafers (Ref) were employed. The samples were fabricated by deep reactive-ion etching (DRIE) (Center for Microtechnologies ZFM, University of Technology Chemnitz, Germany) on silicon wafers and coated with an additional 100 nm titanium (Ti) layer, as reported before [5,7]. Stochastic rough titanium surfaces (corundum-blasted, Ti–CB) and polished titanium (Ti–P) (disk ø 30 mm) with technical purity (grade 2; DOT GmbH Rostock, Germany) were described by Lüthen et al. [4].

2.2. Osteoblast cell culture

The human osteoblast-like cell line MG-63 (American Type Culture Collection ATCC®, CRL-1427) was used throughout the experiments. In addition, for the indicated investigations the human osteoblast-like cell lines SaOs-2 (ATCC, HTB-85) and U-2Os (ATCC, HTB-96) as well as human primary fetal osteoblasts (hFOB, ATCC, CRL11372) and human primary osteoblasts (hOB, PromoCell, Heidelberg, Germany) were used. MG-63, SaOs-2 and U-2Os were grown in Dulbecco's modified eagle medium (DMEM, Life Technologies GmbH, Darmstadt, Germany) with 10% fetal calf serum (FCS) (Biochrom FCS Superior, Merck KGaA, Darmstadt, Germany) and 1% gentamycin (Ratiopharm GmbH, Ulm, Germany) at 37 °C in a humidified atmosphere with 5% CO_2. hFOB were cultured in Ham's F12 DMEM (Life Technologies GmbH) with 10% FCS (Biochrom FCS Superior, Merck) and hOB were cultured in osteoblast growth medium (PromoCell GmbH) at 37 °C in a humidified atmosphere with 5% CO_2. In all experiments 7000 cells/cm^2 were seeded onto the samples placed in NUNC 4-well dishes (Thermo Fisher Scientific, NUNC GmbH & Co. KG, Langenselbond, Germany) or 6-well plates (Greiner Bio-One International GmbH, Kremsmünster, Austria). Before use, the titanium arrays were washed in 70% ethanol for 10 min and rinsed thrice in PBS (PAA Laboratories, Pasching, Austria). For long-term cultivation, after 48 h a media change was made. Filipin III (Sigma–Aldrich, St Louis, MO, USA) was used as caveolae/lipid raft-inhibitor. For this purpose, MG-63 cells were incubated with 0.5 μg/ml Filipin III in DMEM for 15 min at 37 °C with 5% CO_2 after 24 h cultivation on the Ti surfaces.

For internalization experiments MG-63 cells were incubated with melamine particles 6 μm in size marked with FITC (Sigma Aldrich). For this purpose, cells were seeded on cover glasses and incubated for 1 h at 37 °C and 5% CO_2 to ensure adhesion. Afterwards the cells were incubated with the 6 μm particles with a concentration of 10^5/ml for 24 h.

2.3. Real time-qPCR for mRNA expression analyses

Total RNA was isolated using a NucleoSpin®RNA II kit (Macherey–Nagel GmbH & Co KG, Düren, Germany) that includes the elimination of any genomic DNA by DNase (Macherey–Nagel) treatment. The purity and quantity of the resulting RNA were determined via measurement of the absorbance at 280 nm and 260 nm with the Nano Drop 1000 (Thermo Scientific). 50 ng of total RNA was used for first strand cDNA synthesis using Superscript®II Reverse Transkriptase and Random Primers (Invitrogen AG, Carlsbad, CA, USA). The real time quantitative polymerase chain reaction (RT-qPCR) was performed using TaqMan® Universal PCR Master Mix and TaqMan® gene expression assays for alkaline phosphatase (ALP) (Hs00758162_m1), caveolin-1 (Cav-1) (Hs00971716_m1), collagen type 1 (Col1) (Hs0016404_m1), fibronectin (FN) (Hs00900054_m1), glyceraldehyde-3-phosphate dehydrogenase (GAPDH) (Hs99999905_m1) and osteocalcin (OCN) (Hs01587813_g1) (all Applied Biosystems by Life Technologies GmbH, Darmstadt, Germany) following the manufacturer's instructions. TaqMan® PCR assay for each target gene was performed in triplicates of 4 independent experiments. The PCR was performed with Real-Time PCR Applied Biosystem 7500 and the data were collected and analyzed by the 7500 System SDS Software (Applied Biosystems). Each expression was calculated relative to GAPDH (Δ Ct) and then relative to the references (ΔΔ Ct).

2.4. Western-blotting and densitometric analysis

Immunoblots were performed from total lysates of MG-63 cells, which were cultivated on the Ti arrays for 24 h. The BioPlex cell lysis kit (Bio-Rad Laboratories GmbH, Munich, Germany) was used for the cell lysis. Protein quantification was performed using the Bradford method (Bio-Rad Laboratories GmbH). Total cellular protein was separated by SDS-PAGE (Bio-Rad Laboratories GmbH) and afterwards transblotted to PVDF membranes (Roche Diagnostics GmbH, Mannheim, Germany). Analyses were done for rabbit monoclonal anti-annexin A2 (1:1000), rabbit polyclonal anti-caveolin-1 (1:1000) (New England Biolabs GmbH, Frankfurt/Main, Germany), rabbit polyclonal anti-CD68 (1:300) (Proteintech Group Inc., Chicago, IL, USA), rabbit monoclonal anti-Tyr14 phosphorylated caveolin-1(1:1000) (BD Biosciences, Franklin Lakes, NJ, USA) and mouse polyclonal anti-GAPDH (1:1000) (Santa Cruz Biotechnologies Inc., Dallas, TX, USA). The membranes were incubated with the appropriate primary antibody over night at 4 °C followed by a horseradish peroxidase (HRP)-conjugated secondary antibody

(New England Biolabs GmbH). Primary antibody binding was detected by using a fast chemiluminescent substrate for HRP (Femto Dura West Signal, Thermo Scientific).

For each protein detected 4 independent experiments were performed. Immunoblotting analyses were carried out with ImageLab-ChemiDoc-MP (Bio-Rad Laboratories GmbH) and the densitometric analysis with ImageJ (Wayne Rasband, National Institute of Health). GAPDH as well as the stain free with total protein loading were used as an endogenous control.

2.5. Immunofluorescence staining

Osteoblastic cells were cultured on the Ti arrays for 24 h, washed three times with PBS and then fixed with 4% paraformaldehyde (PFA) (10 min; room temperature, RT) (Sigma–Aldrich). After washing thrice with PBS, the cells were permeabilized with 0.1% Triton X-100 (10 min, RT) (Merck), washed again three times with PBS and blocked with 2% bovine serum albumin (BSA) (Sigma–Aldrich) in PBS (30 min, RT). For actin filament staining, cells were incubated with phalloidine coupled with tetramethyl-rhodamine (TRITC) (5 μg/ml in PBS) (Sigma–Aldrich). The following primary antibodies (diluted in PBS) were used for the immunolabeling at RT for 1 h: monoclonal rabbit anti-annexin A2 (1:15), polyclonal rabbit anti-caveolin-1 (New England Biolabs GmbH) (1:400), polyclonal rabbit anti-CD68 (Proteintech Europe Inc.) (1:25), activated integrin monoclonal mouse anti-CD29 9EG7 (BD Biosciences) (1:100) and monoclonal rabbit anti-Tyr14 phosphorylated caveolin-1 (1:50). Secondary antibody anti-rabbit-IgG-AF488 or anti-mouse-IgG-AF488 (Life Technologies, diluted 1:200 in PBS) was applied for 30 min at RT. For cells treated with 6 μm particles marked with the green fluorescence dye FITC, anti-rabbit-IgG-AF594 (Invitrogen AG, diluted 1:200 in PBS) was used as secondary antibody. Cholesterol staining was performed with 2.5 μg/ml filipin III in PBS for 15 min at RT. Nuclei were stained with a 1 μg/ml 4′,6-diamidino-2-phenylindole (DAPI) solution (Sigma–Aldrich) for 15 min at RT. The samples were embedded with fluoroshield mounting media (Sigma–Aldrich).

2.6. Cholesterol quantification

MG-63 cells were cultivated for 24 h on the Ti arrays. After washing with PBS, the cells were trypsinized and suspended in PBS with Ca^{2+}/Mg^{2+} to stop the trypsinization reaction. A centrifugation at 400 *g* for 5 min was performed and the cells were washed in PBS and fixated with 4% PFA (10 min, RT), again washed with PBS and incubated with 100 μg/ml filipin III in PBS (30 min, RT). A centrifugation at 400 *g* for 5 min was performed after every step. Fluorescence was measured in triplicates of 5 independent experiments in a black 96-well plate (Greiner Bio-One International GmbH) by Tecan Infinity 200 (Tecan Group Ltd., Männedorf, Switzerland) with λex = 360 nm and λem = 480 nm.

2.7. ATP and ADP measurement

MG-63 osteoblasts were cultured for 24 h on the Ti samples. Adenosine triphosphate (ATP) measurements were determined using the ATP colorimetric/fluorometric assay kit (Abcam, Cambridge, MA, USA) and adenosine diphosphate (ADP) with ADP colorimetric/fluorometric assay kit (Abcam). Measurements were performed using the fluorometric assay following the manufacturer's instructions. Fluorescence was measured in triplicates in a black 96-well plate by Tecan Infinity 200 (6 independent experiments for the micro-pillared surfaces, 4 independent experiments for Ti–P and Ti–CB disks as well as for the particle-treated cells) with 5×10^4 cells for the Ti arrays and with 1.5×10^5 for the 6 μm particle treatment as well as the polished (Ti–P) and corundum-blasted titanium (Ti–CB) disks for each triplicate. Therefore 3 technical Ti array replicates were pooled.

2.8. Mitochondrial activity

The potential-sensitive fluorescence dye JC-1 (5,5′,6,6′-tetrachloro-1,1′,3,3′-tetraethylbenzimidazolyl-carbocyanine iodide) (Life Technologies GmbH) was used to measure the activity of mitochondria [15]. The dye was dissolved to a stock concentration of 2.5 mg/ml in DMSO. MG-63 cells were cultivated for 24 h on the Ti arrays and then stained with 10 μg/ml JC-1 in DMEM for 15 min at 37 °C in a humidified atmosphere with 5% CO_2. Afterwards the cells were rinsed twice with PBS and the fluorescence was immediately acquired with the inverted laser scanning microscope LSM 780 (Carl Zeiss AG) using a 20× (EC Plan-Neofluar) objective (Carl Zeiss AG). Therefore the Ti arrays were placed into an IBIDI μ-Dish$^{35\ mm,\ high}$ (Ibidi LCC, Martinsried, Germany) with the adherent cells towards the bottom of the dish containing 2 ml of PBS. Green fluorescence was observed through the bandpass of 493–578 nm and red fluorescence through 568–712 nm. Red/green fluorescence was measured with the ZEN 2011 (black version) software (Carl Zeiss AG) by collecting the individual green and red fluorescence of 150 cells at each surface of 2 independent experiments.

2.9. Reactive oxygen species (ROS) determination

Intracellular ROS generation was assessed by using 2′,7′-dichlorofluorescein diacetate (DCF-DA) (DCF-DA cellular ROS detection assay kit, Abcam). MG-63 cells were cultivated for 24 h on the Ti surfaces. After washing with PBS, the cells were trypsinized and resuspended in PBS with Ca^{2+}/Mg^{2+} (PAA Laboratories). A centrifugation at 400 *g* for 5 min was performed; the cells were washed again with PBS followed by another centrifugation step. Subsequently the cells were resuspended in a 20 μM DCF-DA solution and incubated for 30 min at 37 °C in the dark. Positive control was treated with 50 μM tert-butyl hydrogen peroxide for 1 h before staining. ROS in the cells cause oxidation of DCF-DA, yielding the fluorescent product 2′,7′-dichlorofluorescein (DCF). The DCF fluorescence was measured in the flow cytometer FACSCalibur (BD Biosciences, excitation 488 nm). For data acquisition and analyses the software CellQuest Pro 4.0.1 (BD Biosciences) was used and results of 4 independent experiments were presented as arbitrary units (mean channel) of fluorescence intensity.

ROS composition enzymes were quantified as follows: MG-63 cells were cultivated for 24 h on the Ti arrays. The total protein lysis was performed as described for the immunoblots. Protein concentrations were measured using the Bradford method. For the quantification of the ROS composition enzymes Catalase (Cat), Superoxide dismutase (SOD) 1 and SOD2, Peroxiredoxin 2 (PRX2) and Thioredoxin (TRX1) the magnetic bead luminex kit Human Oxidative Stress Magnetic Bead Panel (H0XSTMAG-18K) (Merck KGaA) and the BioPlex 200 system (Bio-Rad Laboratories GmbH) was used following the manufactures' instructions.

2.10. Confocal laser scanning microscopy

The image acquisitions of fixed and vital cells were performed on an inverted confocal laser scanning microscope LSM 780 (Carl Zeiss AG, Oberkochen, Germany). The ZEISS oil immersion objective (C-Apochromat63) and the ZEN 2011 (black version) software (Carl Zeiss AG) were used for the image acquisition. All images were displayed as three dimensional (3D) z-stacks (13 stacks with an interval of 1 μm). Experiments were repeated three times and

images were taken from representative cells.

2.11. Scanning electron microscopy

Cells were washed with PBS three times and then fixed with 2.5% glutardialdehyd (Merck KGaA) for 1 h at RT, dehydrated through a graded series of ethanol (30, 50, 75, 90 and 100% for 5, 5, 15, 10 min and twice for 10 min, respectively) dried in a critical point dryer (K 850, EMITECH, Taunusstein, Germany) and then samples were sputtered with gold for 100 s (layer ca 20 nm) (SCD 004, BAL-TEC, Wetzlar, Germany). Scanning electron microscopy (SEM) observations were performed with a DSM 960A (Carl Zeiss AG) and a MerlinVP microscope (Carl Zeiss AG).

2.12. Statistical analysis

Statistical analyses were carried out with GraphPad Prism5 software (GraphPad Software Inc., La Jolla, CA, USA). Results are presented in box plots with medians, quartiles and an interquartile range (IQR) ± 1.5 × IQR. Data analyses were performed using the Mann–Whitney U test. P-values < 0.05 were considered to indicate significant differences.

3. Results and discussion

3.1. Cell phenotype and function on micro-pillared topography

Actin is the essential element of the cytoskeleton, known to have a primal role in diverse cellular processes controlling the functional and morphological behaviors of cells [16]. Changes in the actin cytoskeleton, overall cell morphology, and the cell nucleus dependent on the growth of MG-63 osteoblasts after 24 h on the micro-pillared topography (dimension 5 × 5 × 5 μm, P − 5 × 5) are shown in Fig. 1. The MG-63 osteoblasts exhibited an elongated phenotype on the pillar structures [5,7]. The cells spread out on the top of the pillars and only the filopodia reached out to the bottom of the topography. This was opposite to the planar samples (Ref), where the MG-63 cells showed a randomly oriented, flattened phenotype and attachment with the entire cell body to the surface. Confocal microscopy with three dimensional (3D) z-stack generation was applied to visualize the short compact actin filaments on the pillar plateaus as well as the actin formation in between the pillars. Z-stacking was used to generate a 3D representation and to understand the overall cell structures not limited to one horizontal plain of the micro-topography, e.g. the top of the pillars. Thus a false interpretation due to different observation levels (confocal principle) could be avoided. The micro-pillars drastically altered the actin cytoskeleton organization of MG-63 cells (Fig. 1a), resulting in clustered and short filaments on the pillar top, as already shown by our group [5,7]. The question remained why the cells rearrange the cytoskeleton in this manner although the actin stress fibers could span from one pillar to the next.

Already on the mRNA level the expression of the osteoblast marker proteins and organic bone matrix components alkaline phosphatase (ALP), collagen type I (Col1), fibronectin (FN) and osteocalcin (OCN) displayed a significant reduction in MG-63 osteoblasts cultured for 24 h on the micro-pillars (Fig. 1b). On the protein level Col1 and FN was shown to be impaired in MG-63 osteoblasts after 24 h on micro-pillared textures already in Refs. [2,7].

Microscopic analysis revealed a nucleus deformation when growing on the micro-pillars (Fig. 1c) as observed by Badique et al. [17] with dimension ranging from 2 to 20 μm for pillar diameter and distances. The nucleus embedded the pillars, leading to a less rounded shape. The sinking down and embedding of the pillars by the nucleus may be caused by fewer prominent, thick actin stress fibers localized above the nucleus in the MG-63 cells. Deformation of the cell nucleus by micrometric surface features has been shown to modify gene expression [18]. However, Badique et al. [17] found no changes in gene expression of osteoblast-specific genes (including Col1) in MG-63, SaOs-2 and OHS-4 osteoblast-like cells despite the deformation of nuclei caused by growth on micro-pillars.

3.2. Attempted phagocytosis – existence of caveolae

Phagocytosis can be mediated via caveolae; therefore we determined the existence of caveolae. The two major caveolae components Cav-1 and cholesterol were localized by immunofluorescence labeling or by interaction with the fluorophore filipin III, respectively (Figs. 2 and 3). Cav-1 displayed a dot-like localization on the micro-pillar plateaus after 24 h of cultivation (Fig. 2a). Tyrosine 14 of caveolin-1 undergoes regulated phosphorylation (pCav-1) presumed by Src family kinases and it is involved in stabilizing the focal adhesion kinase (FAK) at focal adhesion sites (FA) [19]. Several components involved in focal adhesion assembly are also important for phagocytosis and resulting actin reorganization [10]. After 24 h cultivation pCav-1 was augmented at the pillar edges and pillar walls, whereas it was regularly distributed on the reference (Fig. 2a). Protein expression analysis of Cav-1 by western blot revealed a trend towards a decrease of Cav-1 after 24 h on the micro-pillars but an enhanced signal in pCav-1 indicating an elevated phosphorylation state of Cav-1 after 24 h (Fig. 2c). Perhaps in compensation, the Cav-1 mRNA expression was significantly elevated (Fig. 2b). Cav-1 phosphorylation has been linked to caveolar endocytosis [11]. Cholesterol as second major caveolae component also displayed a dot-like formation on the micro-pillar plateaus (Fig. 3). The dot-like locations of Cav-1 (Fig. 2a) and cholesterol (Fig. 3a) imply the local existence of caveolae/lipid rafts, which was not seen on the planar surfaces. To prove the existence of caveolae formation on top of the micro-pillars, cells were treated with the caveolae/lipid raft inhibitor Filipin III (which stains cholesterol, but also acts as inhibitor; in the latter case the cells were incubated with Filipin III before fixation and staining) [13]. The dot-like cholesterol formation on top of the micro-pillars started to disappear; this was accompanied by the disruption of the caveolae/lipid rafts (Fig. 3a). Thus, the dot-like Cav-1 and cholesterol enrichments on top of the pillars revealed caveolae formation. Variation of the pillar sizes (length × width × height × spacing: 1 × 1 × 1 × 1 μm; 2 × 2 × 5 × 2 μm; 3 × 3 × 5 × 3 μm) showed as well a dot-like Cav-1 clustering around and on the pillars after 24 h by MG-63 cells (Fig. 4).

Clustering of lipid rafts/caveolae helps establish polarized platforms necessary for cell adhesion and migration [11]. On the top of the pillars the membrane curvature is positive, which is unfavorable for the accumulation of adhesion molecules in FAs. In addition the membrane experiences strong electrostatic interactions at the pillar plateaus leading to increased membrane tension [20,21]. The normal size of caveolae is about 50–80 nm [11,12]. Bigger caveolae structures emerged on the pillar plateaus (Fig. 2a) and this indicated a formation of multi-caveolar structures, which might allow a greater expansion of the cell surface by coalescence of several small caveolae [11]. Caveolae are reported to act as mechanotransducers in regions with tension generation like the pillar topography [18,22]. As a response to increased surface tension, cholesterol accumulated and increased the thickness as well as stiffness of the membrane lipid bilayers on the pillar plateaus. Accordingly, caveolae incurrence is important for cell adhesion on the micro-pillared topography with reduced adhesion sites. But this does not explain why the actin cytoskeleton was constantly fortified as

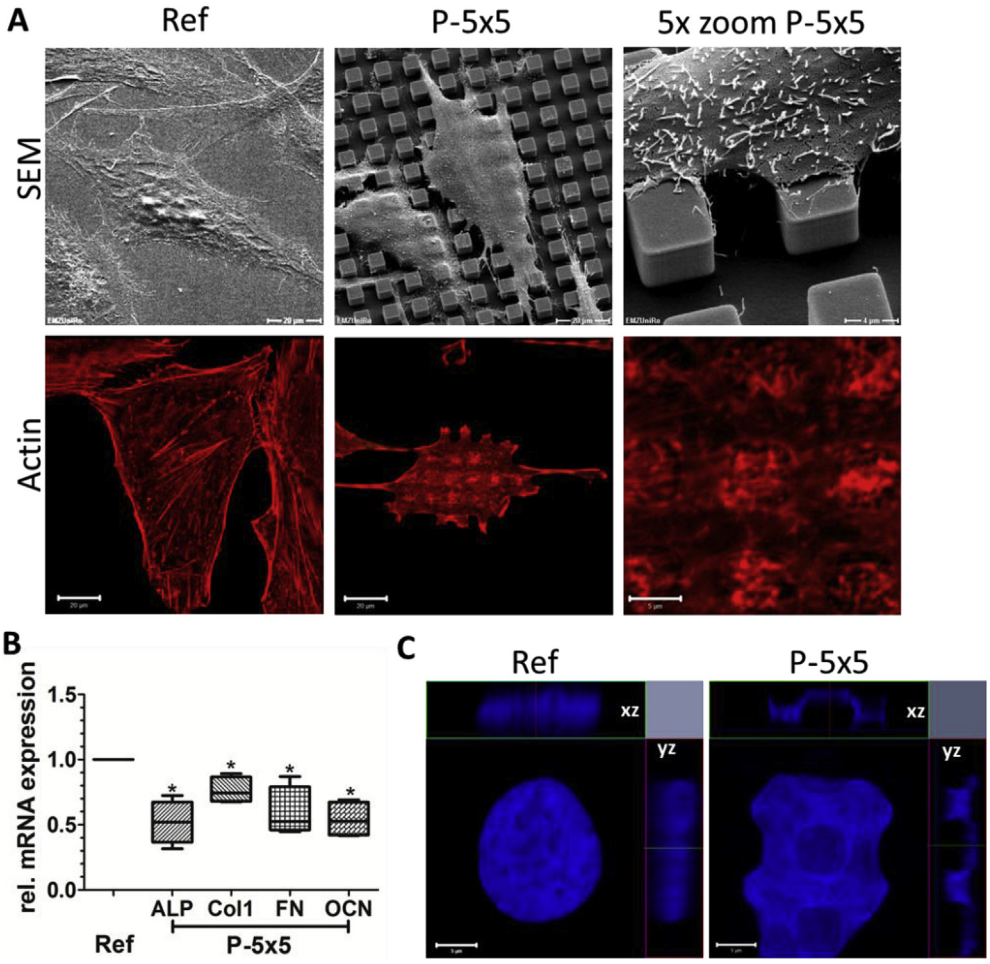

Fig. 1. Morphology and function of MG-63 cells on planar (Ref) and micro-pillared (P – 5 × 5) topography after 24 h. (A) First row: SEM-images (left and middle: 1000× magnification, bar 20 μm; right: 5000× magnification, bar 4 μm, P – 5 × 5 30° twisted, SEM DSM 910); second row: actin cytoskeleton (left and middle bar 20 μm, right 5 μm). (B) Relative mRNA expression of the osteoblastic marker proteins alkaline phosphatase (ALP), collagen type-I (Col1), fibronectin (FN) and osteocalcin (OCN) (Ref values normalized on 1, n = 4, *: P < 0.05). (C) DAPI nuclei staining with xz- and yz-planes. Note that all immunofluorescence images are 3D confocal z-stacks.

short filaments on the pillars and the pillar edges.

Caveolae are known to be semi-permanent and stable membrane structures, so the short actin-filaments on the pillar plateaus should be nonrelevant to keeping the caveolae in a dispersed state [14]. After adhesion and caveolae formation the cells could develop actin stress fibers for stabilization and thus there is no more necessity for the caveolae to act as membrane tension regulators. Actin stress-fiber formation is regulated by membrane cholesterol through processes that require the small GTPase Rho, the kinases ROCK and Src and as well as Cav-1. Cholesterol depletion was shown to enhance stress fiber formation in osteoblasts by increasing the phosphorylation of Cav-1 via Src-family kinases [23]. In our experiments a decline of cholesterol in MG-63 osteoblasts on the micro-pillars (Fig. 3b) could be observed by relative quantification of cellular cholesterol content via Filipin III. Increased Cav-1 phosphorylation (Fig. 2c) was also observed but no actin stress fiber formation. So the cells must underlie another cellular response because normally the regulation of synthesis, influx and efflux keeps cellular cholesterol precisely controlled [24].

Long-term studies over 96 h revealed MG-63 cells reaching to the bottom of the micro-pillared topography and embedding the micro-pillars, visualized by SEM (Fig. 5a). After 96 h on the micro-pillars, the osteoblasts indicated no actin stress fiber formation spanning through the cell and still Cav-1 clustering on the pillar plateaus (Fig. 5b). The actin cytoskeleton started to engulf the pillar walls and the dot-like Cav-1 clusters moved to the pillar edges (Fig. 5b), hinting at phagocytosis of the micro-pillars by the formation of an actin cytoskeleton and Cav-1 coat around the micro-pillars.

Caveolae formation on the pillar plateaus was not exclusively observed in the MG-63 osteoblasts but also in the human osteoblast-like cells SaOs-2 and U-2Os as well as in primary human osteoblasts and fetal osteoblasts (Fig. 6).

3.3. Particle uptake

Caveolae/lipid rafts are associated with the phagocytosis of micron-sized titanium particles [25]. Based on the hypothesis that MG-63 cells attempt to phagocytize the micro-pillars, we wanted to clarify if they are also able to internalize particles of the size of our micro-pillars. The immunofluorescence and SEM images in Fig. 7 showed that the MG-63 cells internalize particles 6 μm in size after 24 h of cultivation. Fig. 7a revealed a complete engulfment of the 6 μm particles with actin by the MG-63 osteoblasts. For verification of the internalization, the immunofluorescence of the x-z and y-z axis as well as 3D z-stack pictures were listed. Not only the actin cytoskeleton but also Cav-1 surrounded the whole particle. These formed caveolin coats around the internalized particle allows us to

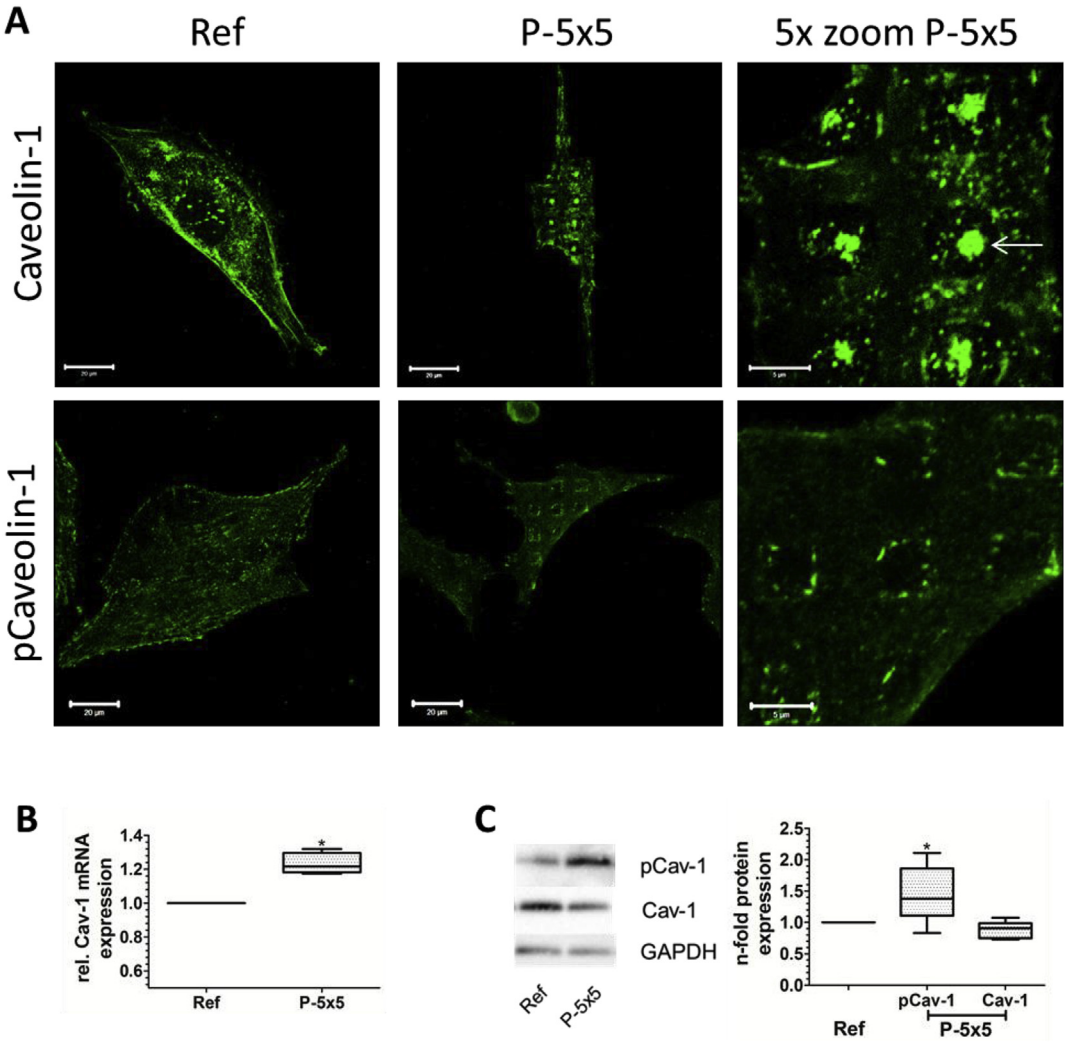

Fig. 2. Caveolin-1 (Cav-1) expression of MG-63 cells on the pillared (P – 5 × 5) and planar (Ref) surfaces after 24 h. (A) First row: Cav-1; second row: tyrosin14-phosphorylated Cav-1 (pCav-1) immunofluorescence (left and middle bar 20 μm, right 5 μm). (B) Relative Cav-1 mRNA expression determined by RT-qPCR (n = 4, *: P < 0.05). (C) Relative protein expression of Cav-1 and pCav-1 measured by western blot (left representative western blots, right densitometric analyses, for pCav-1 n = 6 and for Cav-1 n = 4, *: P < 0.05). Note that Cav-1 formed dot-like clusters on the pillar plateaus (arrow) whereas pCav-1 was located at the pillar edges.

assume that the 6 μm particle uptake is a caveolae/raft mediated internalization process. The experiments demonstrated an uptake of several 6 μm particles by the osteoblast-like cells, but after internalization, all particles were concentrated and not freely distributed inside the cells (Fig. 1a and b in Ref. [26]). In this way the cells may reduce the surface-volume ratio of the internalized cargos, which they cannot do with the fixed micro-pillars. Therefore the attempted uptake of the micro-pillars endured longer than 24 h.

Short interfering RNA (siRNA) mediated knockdown of Cav-1 revealed a reduced particle phagocytosis by MG-63 cells, but no complete inhibition of the phagocytosis (Fig. 2 in Ref. [26]), as was reported in the past [12]. The actin cytoskeleton after Cav-1 attenuation was arranged in short filaments around non-internalized particles, which were washed away during the preparation. The cells attempted to phagocytize these particles as well but they were not able to finish the process after the Cav-1 attenuation and 24 h of incubation with 6 μm particles. The MG-63 osteoblasts with siRNA mediated Cav-1 knockdown grown on the micro-pillars indicated the same rearrangement of the actin cytoskeleton as seen in control cells (Fig. 3 in Ref. [26]). In consequence, the altered actin organization on the micro-pillars is independent of Cav-1 itself.

Only particles <15 μm are reported to be phagocytized by osteoblasts [8]; bigger structures remain trapped at the surface and are subjects of so-called “frustrated” phagocytosis [27]. Despite the fact that our micro-pillars have a much smaller diameter then 15 μm, they also induce a trapped “frustrated” phagocytosis or at least before 96 h of cultivation.

Dalby et al. [28] documented an attempted phagocytosis of columns in the nano-range by fibroblasts, which used the filopodia to explore the underlying topography. These fibroblasts had phenotypic similarities to the osteoblasts on the micro-pillars with regard to disrupted actin cytoskeleton, decreased spreading and changes in morphology, including filopodia development to probe the surface topography (see Movie 1 in Ref. [26]). But the observed nano-column endocytosis was via a clathrin-mediated phagocytosis, an internalization process considered used for small cargos [28]. The role of clathrin-mediated phagocytosis in the micro-pillar uptake was investigated and excluded via clathrin immunofluorescence. Clathrin localization revealed no alteration on the 5 μm sized micro-pillars (data not shown). Furthermore Teo et al. [22]

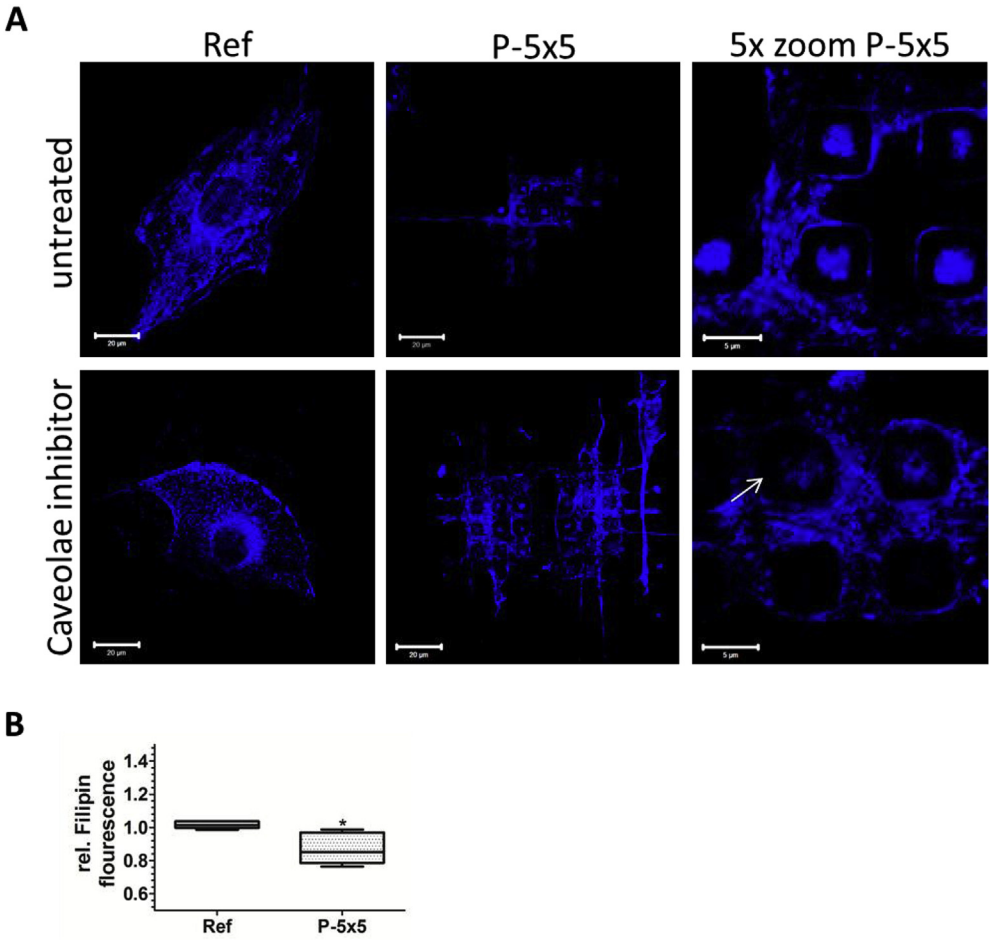

Fig. 3. Cholesterol staining and quantification of MG-63 osteoblasts after 24 h on planar (Ref) and micro-pillared (P–5×5) topographies. (A) First row: cholesterol; second row: cholesterol after pretreatment with filipin III inducing raft/caveolae inhibition (arrow marked the abated dot-like cholesterol formation on the pillar plateaus), (left and middle bar 20 μm, right 5 μm). (B) Relative cholesterol quantification by measurement of filipin III fluorescence (mean value of Ref normalized on 1, n = 5, *: P < 0.05).

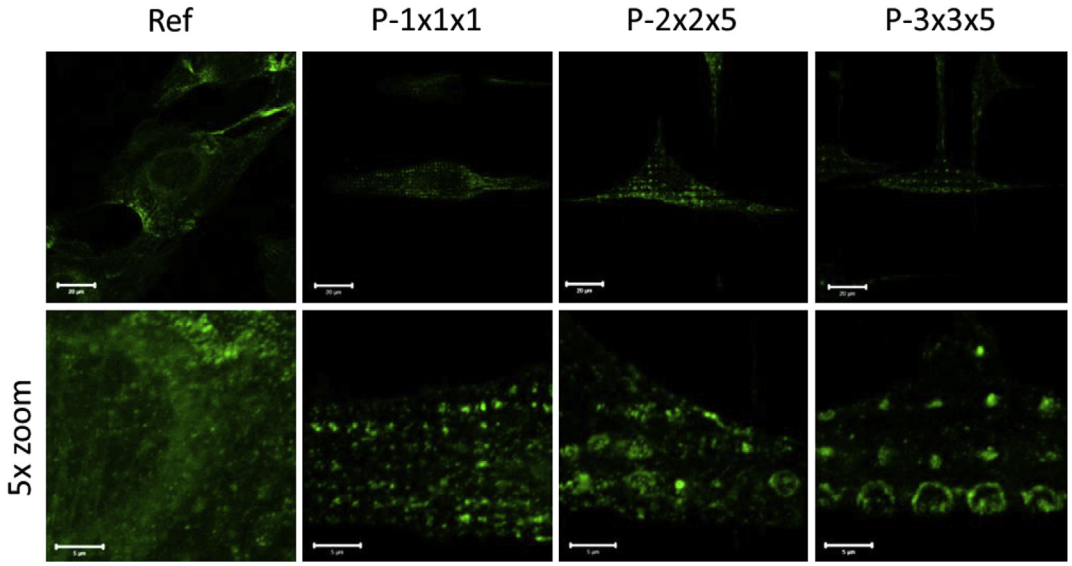

Fig. 4. Caveolin-1 (Cav-1) localization in MG-63 osteoblasts after 24 h on planar surface (Ref) and smaller micro-pillars with the dimensions (width × length × height and spacing) 1 μm×1 μm×1 μm and 1 μm (P–1×1×1); 2 μm×2 μm×5 μm and 2 μm (P–2×2×5); 3 μm×3 μm×5 μm and 3 μm (P–3×3×5) (bar: 20 μm upper row, 5 μm for 5× zoom).

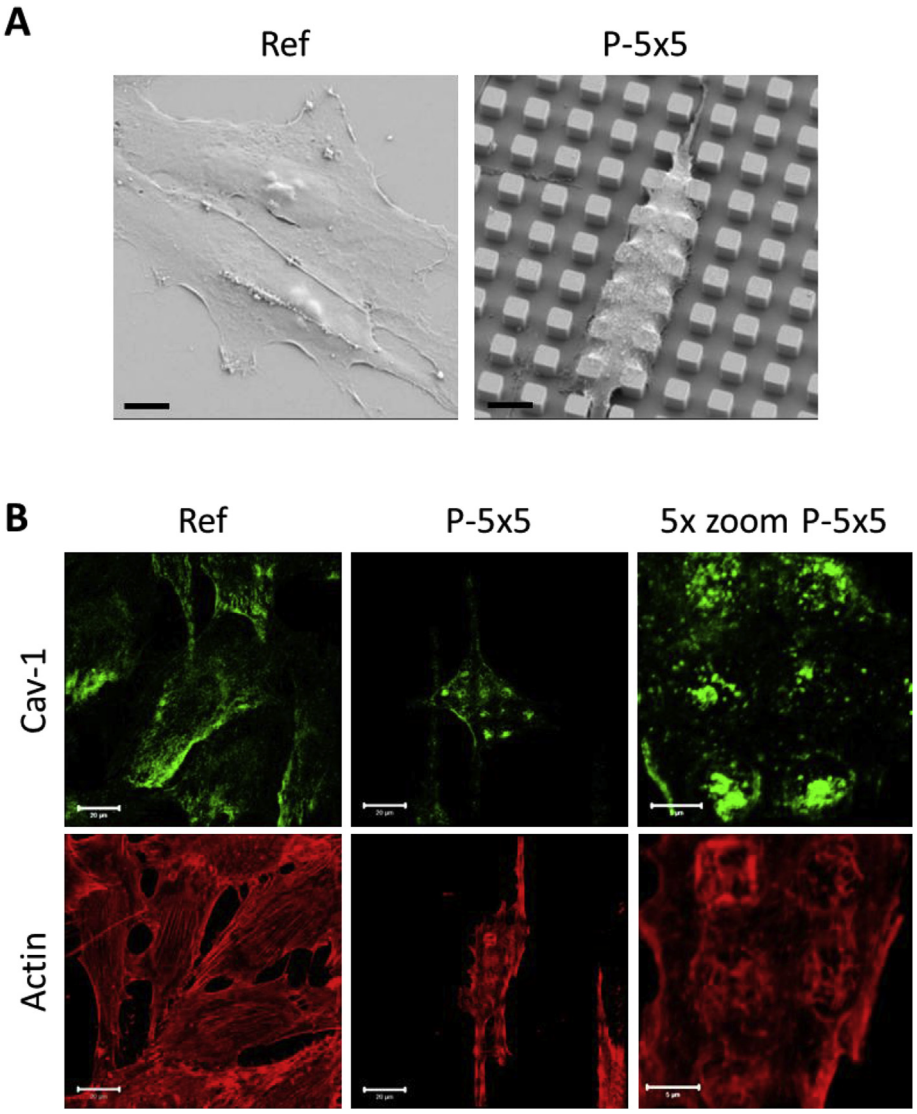

Fig. 5. Cell morphology and caveolin-1 (Cav-1) as well as actin cytoskeleton organization of MG-63 osteoblasts after 96 h of cultivation on planar (Ref) and micro-pillared (P−5×5) surfaces. (A) SEM images (1000× magnification, bars 10 μm, P−5×5 30° twisted, MerlinVP microscope). (B) Cav-1 (green) and actin cytoskeleton (red) immunofluorescence (bar: 20 μm and for 5× zoom 5 μm). (For interpretation of the references to colour in this figure legend, the reader is referred to the web version of this article.)

reported a phagocytosis of 2 μm poly(methyl methacrylate) pillars by human mesenchymal stem cells, the precursor cells of osteoblasts. MG-63 cells are also able to phagocytize particles of various compositions (e.g. titanium, titanium-aluminum-vanadium alloy, cobalt-chrome and ultrahigh molecular weight polyethylene), all leading to a decreased osteoblastic function including reduced Col1 expression, disorganized actin cytoskeleton, and diminished cell spreading and proliferation [8,29–31]. Particle internalization illustrated the local concentration of the internalized cargos by the MG-63 osteoblasts, perhaps in order to decrease the volume-surface ratio of the stored particles inside the cells. This is impossible for the regularly arranged, fixed micro-pillars and may cause

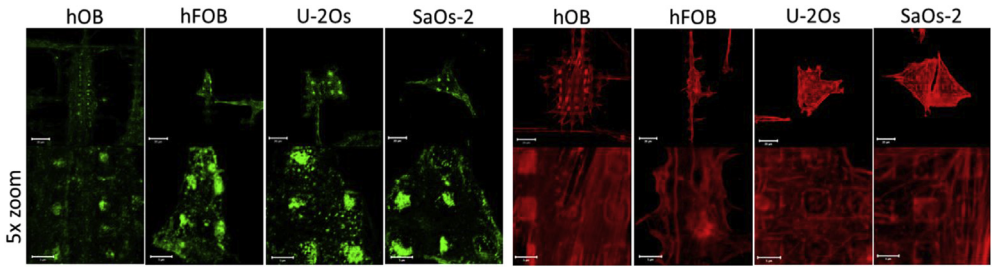

Fig. 6. Caveolin-1 (green) and actin cytoskeleton (red) organization of human primary osteoblasts (hOB), human fetal osteoblasts (hFOB), U-2Os and SaOs-2 osteoblast-like cells after 24 h on the micro-pillars P − 5 × 5 (bar: first row 20 μm and second row 5 μm). (For interpretation of the references to colour in this figure legend, the reader is referred to the web version of this article.)

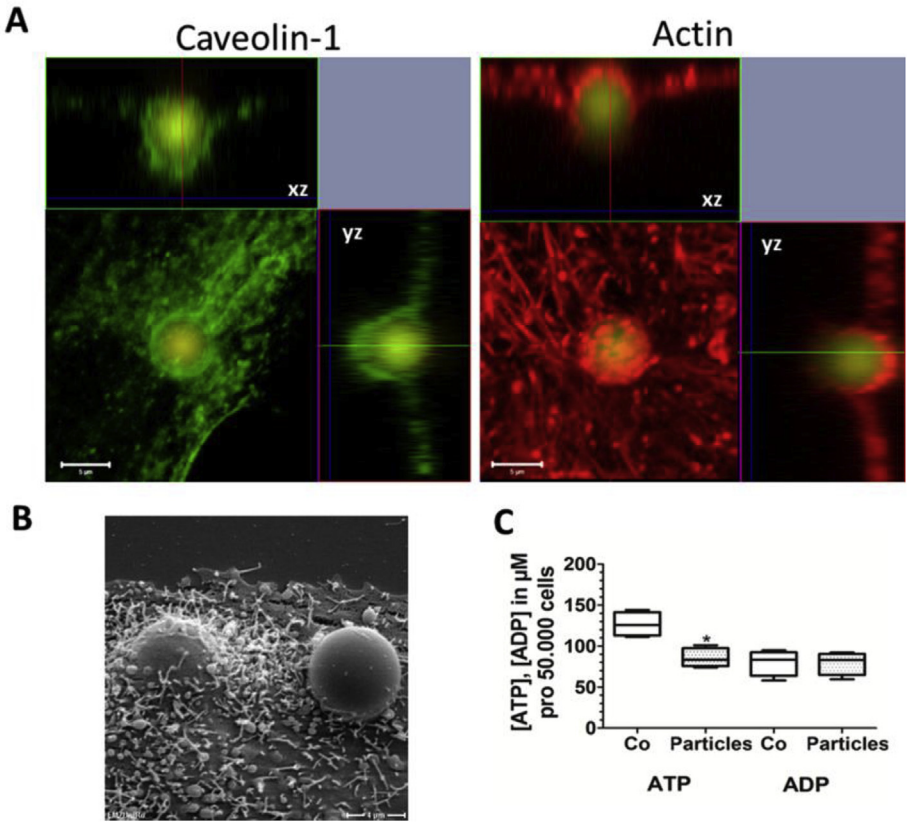

Fig. 7. Particle internalization as well as ATP/ADP quantification after 6 µm melamine FITC-labeled particles treatment of MG-63 osteoblasts for 24 h. (A) Left caveolin-1 (Cav-1, green) and right actin cytoskeleton (red) immunofluorescence with xz-, yz-planes, bars 5 µm. (B) SEM images (5000× magnification, bar 4 µm, DSM 910). (C) Intracellular ATP and ADP quantification (n = 4, *: P < 0.05). Note that the particles were engulfed with a Cav-1 and actin coat.

the termination or deceleration of the uptake process. The internalization of the micro-pillars by the osteoblasts would require a lot of energy and the fixed pillar arrangement does not afford the possibility of concentrating the internalized cargos, as the cells can with particles. This might be the reason for the uncompleted micro-pillar internalization after 4 days.

3.4. Attempted phagocytosis — ATP and ROS

Phagocytosis is known to be a high energy-consuming process, therefore we analyzed the amounts of adenosine triphosphate (ATP) and adenosine diphosphate (ADP) in cells grown on the micro-pillars (Fig. 8) as well as stimulated with 6 µm particles as phagocytosis-triggers. Both showed significant decreases in their cellular ATP and no changes in their ADP levels compared to untreated cells or cells on the planar surface (Ref) (Figs. 7c and 8a). Accordingly, while growing on the micro-pillar topography the osteoblast were metabolizing more ATP compared with cells growing on the planar surface. The same effect was visible after treatment with a phagocytic trigger. Because phagocytosis is an ATP-consuming process in various cell types, including mouse macrophages and rat pheochromocytoma cells, their cellular ATP levels decrease and reactive oxygen species (ROS) production increases, e.g. in response to mobile particles [32,33].

The cells' process of converting energy into ATP is called oxidative phosphorylation and involves the transport of electrons through a series of protein complexes in the mitochondria; this causes the greatest amount of ROS production [34]. On micro-pillared surfaces MG-63 osteoblasts exhibited elevated ROS levels compared to the cells on the planar samples (Fig. 8b) and in accordance with this an increased mitochondrial activity (Fig. 8c). Internalization of particles is also associated with increased ROS, but under most physiological conditions generated ROS are rapidly eliminated by antioxidant enzymes, e.g. Catalase and Superoxid Dismutase [33]. Catalase showed significantly increased protein expression in MG-63 cells grown for 24 h on the micro-pillars (Fig. 8d). Superoxide Dismutase 2 (SOD2) as well as Peroxiredoxin 2 (PRX2) displayed tendential elevations. Cells stabilize their energy charge by adjusting the rate of cellular ATP synthesis to the state of energy demand, but if a process requires high energy, other energy expenditures must be abated [35]. Altogether we assume a high energy requirement for the cell's attempted process of phagocytosis on every single pillar in a fixed position.

3.5. Attempted phagocytosis — phagocytic and raft proteins, β_1-integrin and actin

CD68, a lysosome-associated membrane glycoprotein (LAMP) family member, was found in vesicles of phagocytized particles in osteoblastic cells [29]. As a result, this protein is localized in regions of phagocytic activity [36]. Immunofluorescence staining showed an enrichment of CD68 on the pillar plateaus of the micro-structured surface (Fig. 9a) as well as around internalized particles 6 µm in size (Fig. 4 in Ref. [26]). Enrichment of CD68 at the pillar plateaus is further evidence of the attempt of micro-pillar phagocytosis by the MG-63 cells. But experiments of CD68 protein expression (Fig. 9a) showed a slight decrease of the amount of CD68 protein in cells on micro-pillars. CD68 plays a role in the

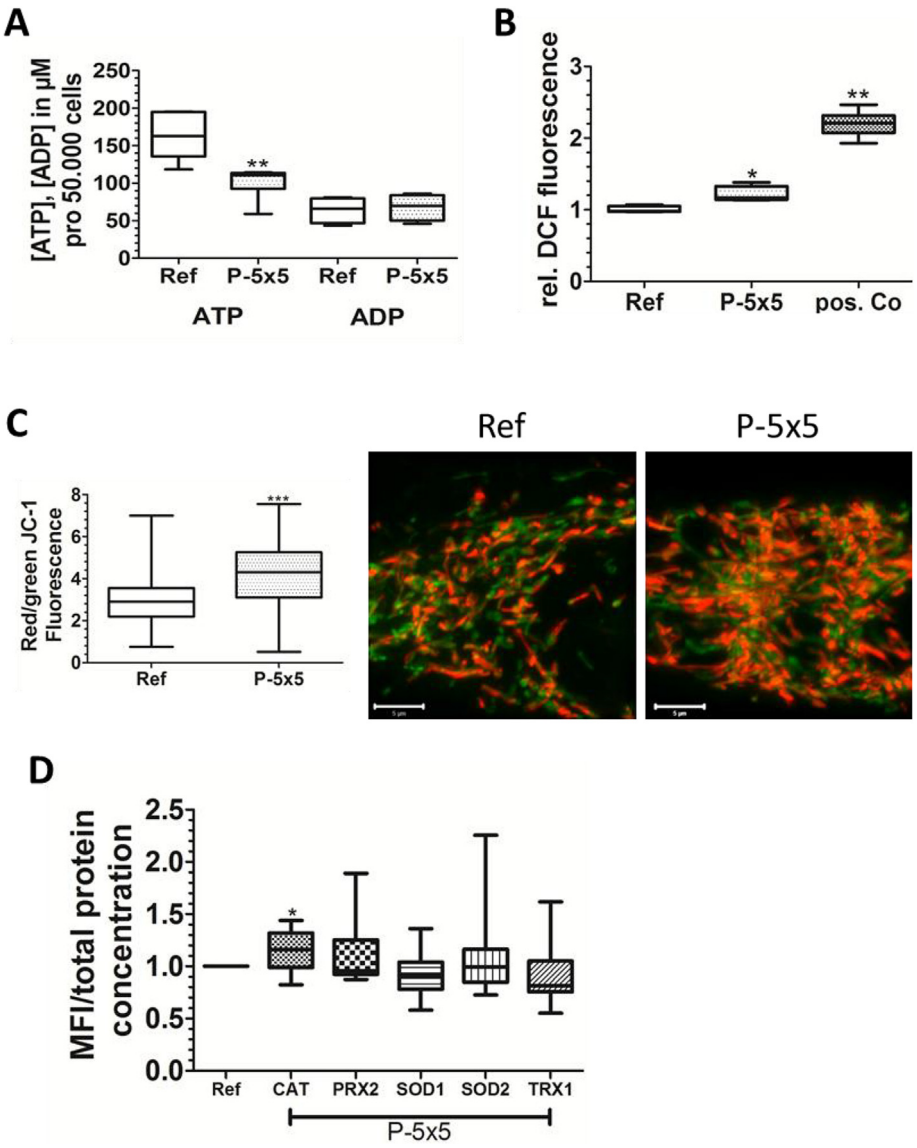

Fig. 8. ATP/ADP level, reactive oxygen species (ROS), mitochondrial activity and ROS composition enzymes in MG-63 osteoblasts after 24 h on planar (Ref) and micro-pillared (P – 5 × 5) surfaces. (A) Intracellular ATP and ADP quantification (n = 6 for ATP, n = 4 for ADP, **: $P < 0.01$). (B) ROS determination (treatment with tert-butyl hydrogen peroxide served as positive control, measurement of 2′,7′-dichlorofluorescin fluorescence (DCF), mean value of Ref normalized on 1, n = 4, *: $P < 0.05$, **: $P < 0.01$). (C) Mitochondrial activity measured by calculating the red/green fluorescence ratio of the mitochondrial membrane potential dye JC-1 (left: n = 2 with à 150 cells, ***: $P < 0.001$, right: images of the stained mitochondria). (D) Expression of ROS composition enzymes Catalase (Cat), Peroxiredoxin 2 (PRX2), Superoxide Dismutase 1 and 2 (SOD1 and SOD2) as well as Thioredoxin 1 (TRX1). Protein quantification was performed with magnetic bead luminex assay (n = 8, *: $P < 0.05$, MFI: mean fluorescence intensity).

delivery of lipids to their proper compartments [36]. We assume that the reduced cellular cholesterol level may resulted by reduced lipid delivery processes accompanied by the high energy-consuming process of the micro-pillar phagocytosis.

AnxA2 is reported to stabilize caveolae but also to bind and recruit actin to the micro-domains [37]. Western blot experiments revealed significantly elevated AnxA2 protein amounts in the osteoblasts on the micro-structured surfaces after 24 h (Fig. 9b). In contrast, immunofluorescence labeling displayed an accumulation of AnxA2 in cells after 3 h on the pillar plateaus but no changes of AnxA2 localization after 24 h in cells on the pillars compared to those on planar references. This might be caused by AnxA2 properties to induce larger cholesterol cluster formation and stabilize caveolae during their formation [37] and after 24 h the caveolae were already formed and needed no further stabilization. AnxA2 is associated with the organization of lipid rafts at sides of actin recruitment [38]. Therefore membrane rafts, as well as caveolae as a special form of lipid rafts, contain proteins and lipids that are involved in the regulation of actin rearrangements at these sides. Plasma membrane reorganization works in concert with the underlying actin cytoskeleton to mediate morphological changes [39]. Actin is also necessary for the attempt to phagocytize [27], and its remodeling is especially sensitive to signals that are generated at the membrane-cytoplasm interphase [40]. Internalization signals cause local tyrosine phosphorylation of proteins leading to a complex series of changes in the caveolae and the actin cytoskeleton, starting with the disassembly of filamentous actin and followed by the recruitment of actin as patches to the cytosolic surface of the caveolae [12], such as the short clustered filaments observed on the pillar plateaus. Regulation of actin-mediated phagocytosis

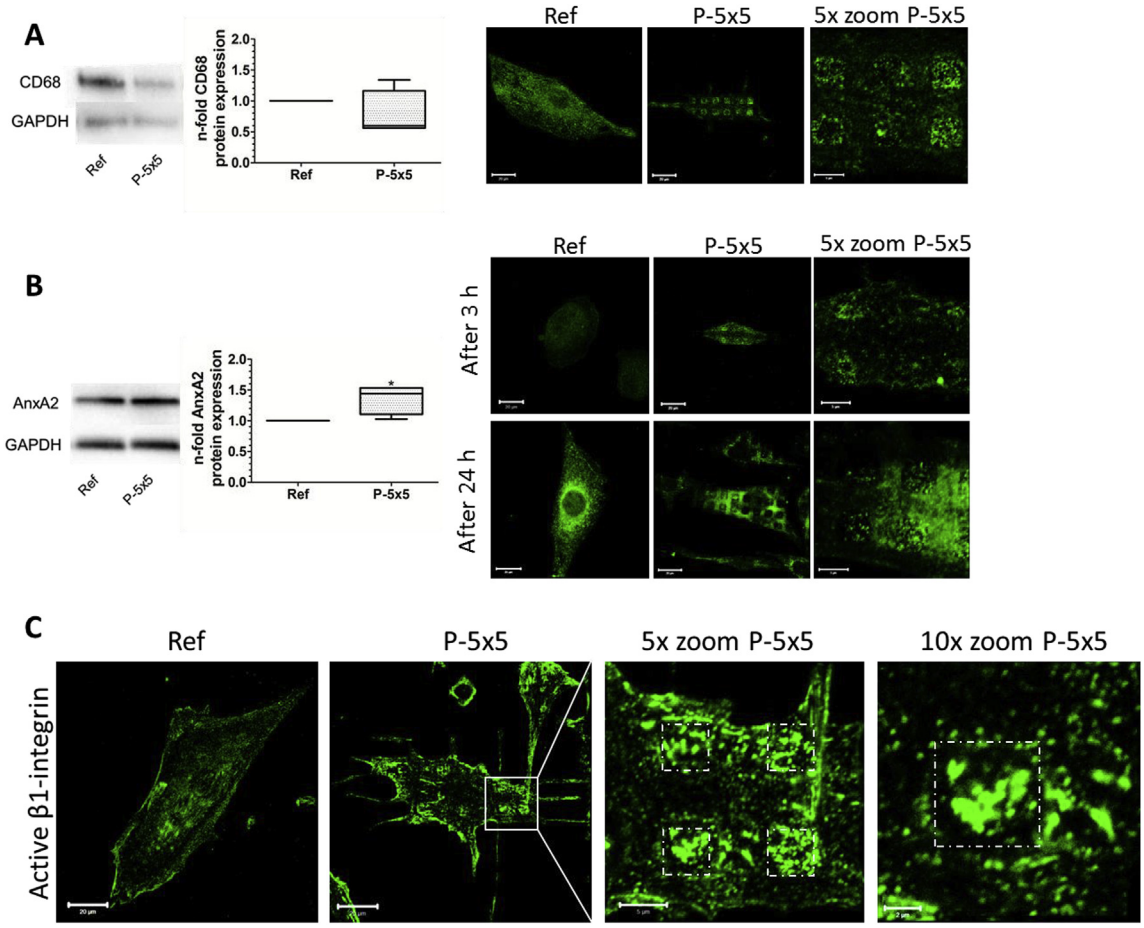

Fig. 9. Analysis of the endocytic protein CD68 and the caveolae-localized protein AnxA2 as well as β1-integrin in MG-63 cells on planar (Ref) and micro-pillared (P − 5 × 5) topographies after 24 h. (A) Left: CD68 protein quantification by western blot and densitometric analysis (Ref values normalized on 1, n = 4). Right: CD68 immunofluorescence (left and middle bar 20 μm and right 5 μm). (B) Left: AnxA2 protein quantification by western blot and densitometric analysis (Ref values normalized on 1, n = 4). Right: AnxA2 immunofluorescence after 3 and 24 h (bars: 20 μm and for 5× zoom 5 μm). (C) CD29 9EG7 (activated β1-integrin) immunofluorescence (zoom region: white square, pillar plateaus: dashed lines at 5× and 10× zoom, bars: 20 μm for 1× zoom, 5 μm for 5× zoom, 2 μm for 10× zoom). Note that activated β1-integrin was concentrated at the pillar plateaus.

depends upon Cav-1 and partly by its posttranslational modifications [39], so internalization triggered Cav-1 tyrosine phosphorylation [11,12]; this was found to be increased in osteoblasts growing on micro-pillared textures (Fig. 2c).

Cell adhesion to the ECM is mediated by integrins in FAs. FAs consist of a complex network of the transmembrane integrins and cytoplasmic proteins linking the ECM to the actin cytoskeleton. The β1-integrin subtype can form heterodimers with various α-integrin subunits and is the predominant receptor involved in osteoblast adhesion [41]. Activated β1-integrin immunolabeling indicated clusters of activated β1-integrin on top of the pillars (Fig. 9c). Clustering of activated β1-integrin might result in elevated adhesion strength [16,30] on the reduced surface area, which in the case of the micro-pillared topography were only represented by the micro-pillar plateaus. Furthermore, Cav-1 phosphorylation is mediated via integrin activated tyrosine kinase Src [19,39]. pCav-1, which is required for phagocytosis and is involved in FA turnover, was localized around the pillars (Fig. 2a) [11]. In addition, integrins are known to mediate phagocytosis over a wide range, from uptake of big particles to the capture of smaller cargos like collagen fibrils. Phagocytosis is not considered to be a feature of specialized integrins but rather an extension of their capacity to mediate adhesion, including integrins that mediate binding to ECM components like the β1-integrin. Phagocytosis and adhesion rely on the same integrin-mediated regulatory and signaling mechanism [42]. Integrin-mediated FAK activation is further required for the reorganization of the actin cytoskeleton and for microtubule stabilization [43]. Tubulin organization in MG-63 cells is not altered by the micro-pillared topography (Fig. 5 in Ref. [26]), but the clustered activated integrin may affect the actin organization regarding actin-driven phagocytosis [42].

3.6. Attempted phagocytosis – rough stochastic surfaces

On commercially available corundum-blasted rough titanium (Ti–CB) surfaces [4], characterized by sharp edges and ridges (Fig. 10), osteoblasts adhered only at the elevations (Fig. 10a) and exhibited an irregularly distributed actin cytoskeleton (Fig. 10b), clusters of β1-integrin in the region of edges and a reduced mineralization rate, and hence decreased osteoblast function after the first 24 h of incubation [4]. Cav-1 was also predominantly localized in the region of the edges (Fig. 10b), like the hole elevations and pits created by the blasting process [4]. Cellular ATP and ROS determination of MG-63 osteoblast-like cells on Ti–CB compared with planar, polished titanium surfaces (Ti–P) after 24 h of cultivation showed, analogous to the micro-pillared topographies, a reduced cellular ATP content (Fig. 10c) and elevated ROS levels (Fig. 10d). But the determination of the ADP content revealed a tendential decrease in the ADP levels (Fig. 10c). The cell behavior on Ti–CB is similar to that on the micro-pillared surfaces as well as after treatment with micro-particles. All of this allows us to assume that the osteoblasts try to internalize the rough surface structures

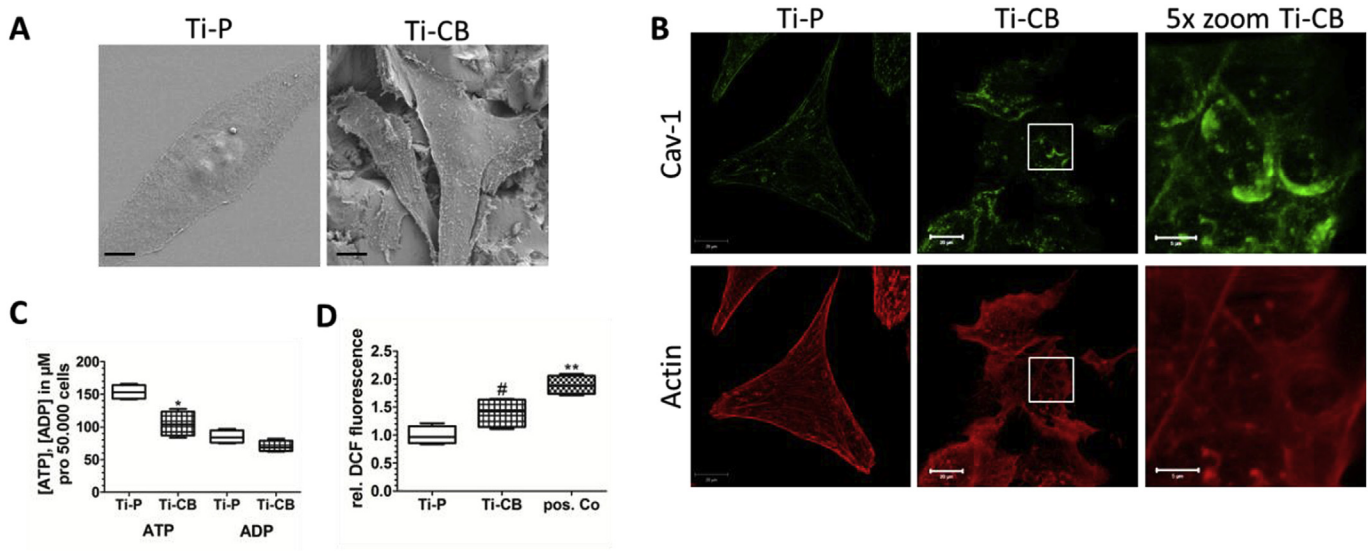

Fig. 10. Influence of the stochastically structured surface Ti–CB (corundum-blasted) vs. Ti–P (polished) on MG-63 cell morphology, reactive oxygen species (ROS) production and energy consumption after 24 h (A) SEM images (1000× magnification, bars 10 µm, P – 5 × 5 30° twisted, MerlinVP microscope). (B) Caveolin-1 (Cav-1; green) and actin cytoskeleton (red) immunofluorescence (bar 20 µm) with 5× zoom of the lined regions (bar 5 µm). (C) Intracellular ATP and ADP quantification (n = 4, *: P < 0.05). (D) ROS determination (treatment with tert-butyl hydrogen peroxide served as positive control, measurement of 2′,7′-dichlorofluorescein fluorescence, mean value of Ti–P normalized on 1, n = 4, #: P = 0.0571; **: P < 0.01). Note the Cav-1 clustering at surface elevations and the similar cell behavior such as on the micro-pillar or treated with 6 µm particles. (For interpretation of the references to colour in this figure legend, the reader is referred to the web version of this article.)

to ensure the maximum ECM contact with the whole cell body and thus maintain osteoblastic function. Because osteoblasts are attachment-dependent cells, the preservation of their osteoblastic function is determined by cell–matrix interactions and the cell's attempt to have maximum contact with the underlying surface [8,43]. MG-63 and the other osteoblasts investigated might attempt to phagocytize the micro-pillars as well for this reason.

Micro-roughness of bone-replacing implants is a controversial factor. Some studies reported positive influences on the osteoblast function and differentiation [44] and others lower cell spreading and osteoblast marker activity [1,3]. Roughening of Ti is used for commercial implants because it provides more surface sides for osseointegration and thus a better mechanical bone fixation [1]. Anselme et al. [3] reported that human osteoblasts prefer surfaces with moderate micro-roughness but with a low level of repeatability concerning their orientation, adhesion and proliferation. According to the knowledge gathered in this study, surfaces that offer the osteoblastic cells insufficient ECM interaction area and in consequence induce internalization processes lead to a decrease in the cells' osteoblastic function. These osteoblasts exhibit impaired biomaterial interaction in the first phase of osseointegration, which would lead to a decrease in acceptance and success of an implant [1].

Micro-pillar topographies, ineligible as implant design, allow modulation of cytoskeletal arrangements; they affect adhesion and proliferation as well as induce differentiation of osteoblasts [2,5,17,22]. This topography may provide another way of eliciting responses that could be exploited for research tools and medical materials. Due to this geometrical arrangement of surface features we could reveal the reason why cells organize their actin cytoskeleton around the elevations leading to the reduced cell function. Thus we suggest that stochastically structured implants used in orthopedic surgery should avoid any topographical heights inducing phagocytosis to prevent their successful ingrowth.

4. Conclusion

This study describes for the first time the attempted caveolae-mediated phagocytosis of fixed, titanium coated micro-pillars by human MG-63 osteoblastic cells and explains the local actin rearrangement in a way which mimics the underlying Ti surface. This attempt to phagocytize the cubic elevations of the Ti surface costs the cells internal energy as indicated by the ATP loss as well as induces an increase of intracellular radicals (ROS). Within the context of the development of new bioactive implant designs, the artificial micro-structured pillar topography used here highlights the importance of the cell-material contact area for the osteoblasts in maintaining their specific osteoblastic function and how this contact can manipulate the cell reactions. Altogether, bone-replacing implant biomaterials should provide (i) sufficient contact area without micron-sized elevations like spikes or sharp edges that induce internalization by the osteoblastic cells and consequently impair their osteoblastic function and (ii) enough surface sides or area to provide a good mechanical fixation of the implant in the native bone, possibly via macro-roughness in dimensions greater than one cell.

Acknowledgments

We are grateful for the financial support of the DFG Graduate School *welisa* (No. 1505/2) for CM. We thank Norbert Zichner (Center for Microtechnologies ZFM, Chemnitz University of Technology, Germany) for the production of the titanium-coated materials and Marcus Frank (Electron Microscopy Center, University Medical Center Rostock, Germany) for his assistance with electron microscopy. We gratefully acknowledge Alexander D. Bershadsky (Weizmann Institute of Science/Rehovot, Israel and National University of Singapore) for his scientific input and fruitful discussions.

References

[1] L. Bacakova, E. Filova, M. Parizek, T. Ruml, V. Svorcik, Modulation of cell adhesion, proliferation and differentiation on materials designed for body

implants, Biotech. Adv. 29 (2011) 739–767, http://dx.doi.org/10.1016/j.biotechadv.2011.06.004.
[2] C. Matschegewski, S. Staehlke, R. Loeffler, R. Lange, F. Chai, D.P. Kern, U. Beck, B.J. Nebe, Cell architecture – cell function dependencies on titanium arrays with regular geometry, Biomaterials 31 (2010) 5729–5740, http://dx.doi.org/10.1016/j.biomaterials.2010.03.073.
[3] K. Anselme, M. Bigerelle, B. Noël, A. Iost, P. Hardouin, Effect of grooved titanium substratum on human osteoblastic cell growth, J. Biomed. Mater. Res. 60 (4) (2002) 529–540, http://dx.doi.org/10.1002/jbm.10101.
[4] F. Lüthen, R. Lange, P. Becker, J. Rychly, U. Beck, J.B. Nebe, The influence of surface roughness of titanium on β1- and β3-integrin adhesion and the organization of fibronectin in human osteoblastic cells, Biomaterials 26 (2005) 2423–2440, http://dx.doi.org/10.1016/j.biomaterials.2004.07.054.
[5] C. Matschegewski, S. Staehlke, H. Birkholz, R. Lange, U. Beck, K. Engel, J.B. Nebe, Automatic actin filament quantification of osteoblasts and their morphometric analysis on microtextured silicon-titanium arrays, Materials 15 (2012), http://dx.doi.org/10.3390/ma5071176, 11776–21195.
[6] E.M. Czekanska, M.J. Stoddart, R.G. Richards, J.S. Hayes, In search of an osteoblast cell model for in vitro research, Eur. Cell Mat. 24 (2012) 1–17.
[7] S. Staehlke, A. Koertge, B. Nebe, Intracellular calcium dynamics dependent on defined microtopographical features of titanium, Biomaterials 46 (2015) 48–57, http://dx.doi.org/10.1016/j.biomaterials.2014.12.016.
[8] M.G. Choi, H.S. Koh, D. Kluess, D. O'Connor, A. Mathur, G.A. Truskey, J. Rubin, D.X.F. Zhou, K.L.P. Sung, Effects of titanium particle size on osteoblast functions in vitro and in vivo, PNAS 102 (12) (2005) 4578–4583, http://dx.doi.org/10.1073/pnas.0500693102.
[9] L.G. Gutwein, T.J. Webster, Osteoblast and chondrocyte proliferation in the presence of alumina and titania nanoparticles, J. Nanopart Res. 4 (2002) 231–238.
[10] R.C. May, L.M. Machesky, Phagocytosis and the actin cytoskeleton, J. Cell Sci. 114 (2001) 1061–1077.
[11] R.G. Parton, M.A. del Pozo, Caveolae as plasma membrane sensors, protectors and organizers, Nat. Rev. Mol. Cell Biol. 14 (2013) 98–112, http://dx.doi.org/10.1038/nrm3512.
[12] L. Pelkmans, A. Helenius, Endocytosis via caveolae, Traffic 3 (2002) 311–320, http://dx.doi.org/10.1034/j.1600-0854.2002.30501.x.
[13] C.J. Fielding, P.E. Fielding, Relationship between cholesterol trafficking and signaling in rafts and caveolae, Biochim. Biophys. Acta 1610 (2003) 219–228, http://dx.doi.org/10.1016/S0005-2736(03)00020-8.
[14] A. Viola, N. Gupta, Tether and trap: regulation of membrane-raft dynamics by actin-binding proteins, Nat. Rev. Immunol. 7 (2007) 889–896, http://dx.doi.org/10.1038/nri2193.
[15] M. Reers, T.W. Smith, L.B. Chen, Mitochondrial membrane potential monitored by JC-1 dye, Methods Enzymol. 260 (1995) 406–414.
[16] M.J.P. Biggs, R.G. Richards, M.J. Dalby, Nanotopographical modification: a regulator of cellular function through focal adhesions, Nanomedicine NBM 6 (2010) 619–633, http://dx.doi.org/10.1016/j.nano.2010.01.009.
[17] F. Badique, D.R. Stamov, P.M. Davidson, M. Veuillet, G. Reiter, J.N. Freund, C.M. Franz, K. Anselme, Directing nuclear deformation on micropillared surfaces by substrate geometry and cytoskeleton organization, Biomaterials 34 (2013) 2991–3001. http://dx.doi.org/10.1016/j.biomaterials.2013.01.018.
[18] L.E. McNamara, R. Burchmore, M.O. Riehle, P. Herzyk, M.J.P. Biggs, C.D.W. Wilkinson, A.S.G. Curtis, M.J. Dalby, The role of microtopography in cellular mechanotransduction, Biomaterials 33 (2012) 2835–2847, http://dx.doi.org/10.1016/j.biomaterials.2011.11.047.
[19] M. Nethe, P.L. Hordijk, A model for phosphor-caveolin-1 driven turnover of focal adhesions, Cell Adhes. Migr. 5 (1) (2011) 59–64, http://dx.doi.org/10.4161/cam.5.1.13702.
[20] D. Kabaso, E. Gongadze, S. Perutkova, C. Matschegewski, V. Kralj-Iglic, U. Beck, U. van Rienen, A. Iglic, Mechanics and electrostatics of the interactions between osteoblasts and titanium surface, Comput. Meth Biomech. Biomed. Eng. 14 (05) (2011) 469–482, http://dx.doi.org/10.1080/10255842.2010.534986.
[21] H.T. McMahon, J.L. Gallop, Membrane curvature and mechanisms of dynamic cell membrane remodelling, Nature 438 (2005) 590–596, http://dx.doi.org/10.1038/nature04396.
[22] B.K.K. Teo, S.H. Goh, T.S. Kustandi, W.W. Loh, H.Y. Low, E.K.F. Yim, The effect of micro and nanotopography on endocytosis in drug and gene delivery systems, Biomaterials 32 (2011) 9866–9875, http://dx.doi.org/10.1016/j.biomaterials.2011.08.088.
[23] M. Qi, Y. Liu, M.R. Freeman, K.R. Solomon, Cholesterol-regulated stress fiber formation, J. Cell Biochem. 106 (2009) 1031–1040, http://dx.doi.org/10.1002/jcb.22081.
[24] K. Simons, E. Ikonen, How cells handle cholesterol, Science 290 (2000) 1721–1726, http://dx.doi.org/10.1126/science.290.5497.1721.
[25] G. Nagao, K. Ishii, K. Hirota, K. Makino, H. Terada, Role of lipid rafts in phagocytic uptake of polystyrene latex microspheres by macrophages, Anticancer Res. 30 (2010) 3167–3176.
[26] C. Moerke, P. Mueller, B. Nebe, Data supporting attempted caveolae-mediated phagocytosis of surface-fixed micro-pillars by human osteoblasts, Data Brief (2015) (submitted).
[27] C. Dostert, V. Petrilli, R. van Bruggen, C. Steele, B.T. Mossman, J. Tschopp, Innate immune activation through Nalp3 inflammasome sensing of asbestos and silica, Science 320 (2008) 674–677, http://dx.doi.org/10.1126/science.1156995.
[28] M.J. Dalby, C.C. Berry, M.O. Riehle, D.S. Sutherland, H. Agheli, A.S.G. Curtisa, Attempted endocytosis of nano-environment produced by colloidal lithography by human fibroblasts, Exp. Cell Res. 295 (2004) 387–394, http://dx.doi.org/10.1016/j.yexcr.2004.02.004.
[29] D.E.H. Heinemann, C. Lohmann, H. Siggelkow, F. Alves, I. Engel, G. Köster, Human osteoblast-like cells phagocytose metal particles and express the macrophage marker CD68 in vitro, J. Bone Jt. Surg. 82 (B) (2000) 283–289.
[30] L. Saldana, N. Vilaboa, Effects of micrometric titanium particles on osteoblast attachment and cytoskeleton architecture, Acta Biomater. 6 (2010) 1649–1660, http://dx.doi.org/10.1016/j.actbio.2009.10.033.
[31] J. Yao, G. CS-Szabo, J. Jacobs, K. Kuettner, T. Glant, Suppression of osteoblast function by titanium particles, J. Bone Jt. Surg. Am. 79 (1) (1997) 107–112.
[32] N. Borregaard, T. Herlin, Energy metabolism of human neutrophil during phagocytosis, J. Clin. Invest. 70 (1982) 550–557.
[33] Y.S. Jeong, W.K. Oh, S. Kim, J. Jang, Cellular uptake, cytotoxicity, and ROS generation with silica/conducting polymer core/shell nanospheres, Biomaterials 32 (2011) 7217–7225, http://dx.doi.org/10.1016/j.biomaterials.2011.06.020.
[34] F. Wauquier, L. Leotoing, V. Coxam, J. Guicheux, Y. Wittrant, Oxidative stress in bone remodeling and disease, Trends Mol. Med. 15 (10) (2009) 468–477, http://dx.doi.org/10.1016/j.molmed.2009.08.004.
[35] F.I. Ataullakhanov, V.M. Vitvitsky, What determines the intracellular ATP concentration, Biosci. Rep. 22 (2002) 501–511.
[36] L. Song, C. Lee C,Schindler, Depletion of the murine scavenger receptor CD68, J. Lipid Res. 52 (2011) 1542–1550.
[37] P. Drücker, M. Pejic, H.J. Galla, V. Gerke, Lipid segregation and membrane budding induced by peripheral membrane binding protein annexin A2, J. Biol. Chem. 288 (34) (2013) 24764–24776, http://dx.doi.org/10.1074/jbc.M113.474023.
[38] V. Gerke, C.E. Creutz, S.E. Moss, Annexins: linking Ca^{2+} signaling to membrane dynamics, Nat. Rev. Mol. Cell Biol. 6 (2005) 449–461, http://dx.doi.org/10.1038/nrm1661.
[39] B.P. Head, H.H. Patel, P.A. Insel, Interaction of membrane/lipid rafts with the cytoskeleton: impact on signaling and function, Biochim. Biophys. Acta 1838 (2014) 532–545, http://dx.doi.org/10.1016/j.bbamem.2013.07.018.
[40] P.A. Janmey, U. Lindberg, Cytoskeletal regulation: rich in lipids, Nat. Rev. Mol. Cell Biol. 5 (2004) 658–666, http://dx.doi.org/10.1038/nrm1434.
[41] P. Kanchanawong, G. Shtengel, A.M. Pasapera, E.B. Ramko, M.W. Davidson, H.F. Hess, C.M. Waterman, Nanoscale architecture of integrin-based cell adhesions, Nature 468 (2010) 580–586, http://dx.doi.org/10.1038/nature09621.
[42] A.G. Dupuy, E. Caron, Integrin-dependent phagocytosis – spreading from microadhesion to new concepts, J. Cell Sci. 121 (2008) 1773–1783, http://dx.doi.org/10.1242/jcs.018036.
[43] L. Saldana, N. Vilaboa, Effects of micrometric titanium particles on osteoblast attachment and cytoskeleton architecture, Acta Biomater. 6 (2010) 1649–1660, http://dx.doi.org/10.1016/j.actbio.2009.10.033.
[44] Z. Schwartz, R. Olivares-Navarrete, M. Wieland, D.L. Cochran, B.D. Boyan, Mechanisms regulating increased production of osteoprotegerin by osteoblasts cultured on microstructured titanium surfaces, Biomaterials 30 (2009) 3390–3396, http://dx.doi.org/10.1016/j.biomaterials.2009.03.047.